Dropdown Analysis of High-Speed Thin-Shaft Coupled Rotor System Integrated with Three Active Magnetic Bearings

Gyan Ranjan(✉), Juuso Narsakka, Tuhin Choudhury, and Jussi Sopanen

Department of Mechanical Engineering, Lappeenranta-Lahti, University of Technology, LUT Skinnarilankatu 34, 53850 Lappeenranta, Finland
{Gyan.Ranjan,Juuso.Narsakka,Tuhin.Choudhury,
Jussi.Sopanen}@lut.fi

Abstract. Rotating machines supported by Active Magnetic Bearings (AMBs) are also equipped with touchdown bearings (TDBs) to support the rotor in cases of power failure or overload of AMBs system. In these dropdown events, the TDBs absorb the impact of the dynamic loads. The simulation and analysis of the orbit responses from such dropdown events can be utilized to prevent critical damage to the machinery. To that end, this study presents the dropdown simulation of a megawatt class induction machine driveline, levitated on three AMBs. The driveline has two AMBs for the motor and one AMB supporting the impeller of a compressor on an extension shaft. The shafts are connected via a thin shaft coupling. The system is first levitated with the designed LQR controller. To simulate a dropdown event, the destabilized system is allowed to fall under the influence of gravity load at the three TDBs. The time domain displacement amplitudes of the FE model are generated for different contact conditions based on the tangential velocity of the rotor. The vibrational amplitudes with different values of unbalance forces are analyzed to identify the most critical bearing and determine the operational limits of rotor system.

Keywords: Active Magnetic Bearings · Dropdown Analysis · High-Speed Rotor · LQR control · Finite Element Method

1 Introduction

The first direct drive high-speed machines were designed for the applications where high power and low mass and volume were required with less emphasis on cost of the machine, such as racing and aeroengines [1, 2]. The first high-speed machines were equipped with conventional roller or sliding bearings. The development of active magnetic bearings (AMBs) has opened the field of machines where frictionless rotational systems are possible. The advantages of a direct high-speed AMB driveline, such as oil-free and low-maintenance operation and a small footprint, have increased interest in more general applications such as compressors, turbines, and pumps. Downside of the direct high-speed machines has been a long development time due to demanding multidisciplinary

F. Chu and Z. Qin (Eds.): IFToMM 2023, MMS 139, pp. 190–200, 2024.
https://doi.org/10.1007/978-3-031-40455-9_15

design process. Also, the nature of case specific design is limiting the usability of same design for various application, which results in small manufacturing batches and high unit costs [3].

To overcome the usability challenge, a novel three radial AMB rotor configuration is proposed to be used in part of the modular high-speed driveline [4]. With the new technical solution is always necessary to study its capabilities from various aspects. The main target of this study is to investigate the performance of touchdown bearings in new rotor configuration. To be able to study the performance of TDBs under different usage situations, a simulation model including the rotor, AMBs and TDBs must be built. From previous studies of TDBs and rotor AMB systems [5–7] can be derived the methods for constructing a simulation in which operational levitation and dropdown event transient analysis can be studied. Also, the analysis of orbit responses at TDBs locations and the design of different AMB controller are important areas of research for rotor-AMB configuration [8–10]. The scope of this work is to analyze the behavior of the three AMB configuration in a dropdown situation, and the influencing parameters for maximum load at TDBs. Also, the critical bearing is identified in different dropdown conditions to avoid failure to the machinery.

The structure of the work is as follows: In Sect. 2 is presented the theory of the simulation model. In Sect. 3, the configuration and case study of the proposed new solution are described. In Sect. 4 are presented the results and analysis of simulation. Sect. 5 includes the conclusion of the work.

2 Mathematical Modelling of Thin-Shaft Coupled Rotor-AMB System with TDBs

The mathematical model of the rotor system is developed using Timoshenko beam elements. The system is analyzed for the lateral vibrations in the axis perpendicular to the shaft axis (z). Two translations and two rotational degrees of freedoms (DoFs) are considered at each node locations. The compressor drive and extension shaft with an impeller are supported on AMBs. A thin-shaft coupling is used to connect the compressor drive with an extension shaft. The rotor system also comprises of TDBs to support the system in case of a dropdown event or when the rotor is not levitated.

2.1 Equations of Motion of Rotor System

The flexible shaft is discretized into several elements and the impeller is added as a rigid disc to the respective location on the rotor. The assembled equation of motion of the rotor system is given as

$$(\mathbf{M}_s + \mathbf{M}_d)\ddot{\mathbf{r}}(t) + (\mathbf{C}_s + \omega(\mathbf{G}_s + \mathbf{G}_d))\dot{\mathbf{r}}(t) + \mathbf{K}_s\mathbf{r}(t) = \mathbf{f}_e(t) + \mathbf{f}_g \tag{1}$$

with,

$$\mathbf{C}_s = \alpha\,(\mathbf{M}_s + \mathbf{M}_d) + \beta\mathbf{K}_s;\ \mathbf{f}_e = me\omega^2 e^{j(\omega t+\theta)}\mathbf{x} \tag{2}$$

where $\mathbf{M}_s$, $\mathbf{C}_s$, $\mathbf{G}_s$ and $\mathbf{K}_s$ are the mass, damping, gyroscopic and stiffness matrices of the shaft. $\mathbf{M}_d$ and $\mathbf{G}_d$ are the mass and gyroscopic matrices of the rigid disc. Proportional

damping matrix (Rayleigh damping) is obtained using coefficients α and β. $\mathbf{f}_g$ is the gravity load vector of the rotor system. $\mathbf{f}_e$ is the unbalance force at the impeller location. m, e, θ are the mass, eccentricity, and phase of the unbalance in the rotor system. ω is the operating speed of the rotor system. $\mathbf{x}$ is the position vector of the unbalance force and is given as

$$\mathbf{x} = [0\,0\,0 \ldots 1 \ldots]^{\mathrm{T}} \tag{3}$$

where, '1' is the location of the unbalance.

2.2 AMB Support System Model

The rotor system is supported on AMBs at different locations. A linearized AMB force model is utilized in the present work with differential driving mode control and is given as

$$\mathbf{f}_a(t) = -\mathbf{K}_a\mathbf{r}_a + \mathbf{K}_i\mathbf{i}_c \tag{4}$$

where, $\mathbf{K}_a$ and $\mathbf{K}_i$ are the displacement and the current stiffness matrices of AMBs. $\mathbf{r}_a$ and $\mathbf{i}_c$ are the displacements at AMB locations and control currents respectively. The controller of the AMB system is designed based on the LQR control strategy. The state space representation of the rotor system is given as

$$\mathbf{A}=\begin{bmatrix} 0 & 1 \\ -\mathbf{M}_m^{-1}(\mathbf{K}_m - K_{\mathrm{a,m}}) & -\mathbf{M}_m^{-1}(\mathbf{C}_m + \omega\mathbf{G}_m) \end{bmatrix} \tag{5}$$

$$\mathbf{B} = \begin{bmatrix} 0 \\ -\mathbf{M}_m^{-1}\,\mathbf{K}_{i,m} \end{bmatrix};\ \mathbf{Q};\ \mathbf{R} \tag{6}$$

where, $\mathbf{M}_m$, $\mathbf{C}_m$, $\mathbf{G}_m$, $\mathbf{K}_m$, $\mathbf{K}_{a,m}$ and $\mathbf{K}_{i,m}$ are the reduced order matrices of the rotor-AMB system with required DoFs to control. The $\mathbf{Q}$ and $\mathbf{R}$ are weights given to states and control vectors [11]. The controller matrix, $\mathbf{H}$ is obtained solving the Algebraic Ricatti Equation. The state space matrix with LQR control is given as

$$\mathbf{A}_e = \mathbf{A} - \mathbf{BH} \tag{7}$$

The AMB force with the LQR control model combined with integral action is given as

$$\mathbf{f}_a(t) = -\mathbf{K}_a\mathbf{r}_a + \mathbf{K}_i\Big(\mathbf{H}\{\mathbf{r}_s\,\dot{\mathbf{r}}_s\}^T + \mathbf{K}_I\bar{\mathbf{r}}_s\Big) \tag{8}$$

where, $\mathbf{K}_I$ is the integral gain of the controller and $\mathbf{r}_s$ is the responses estimated through Kalman observer. $\bar{\mathbf{r}}_s$ is the integration of the estimated responses.

2.3 Touchdown Bearing Force Model

The touchdown bearing forces are modelled based on displacements ($\mathbf{r}_t$) exceeding the air gap (c) between rotor and TDB [6, 12]. The relative responses at

TDBs are given as

$$\mathbf{r}_e = (|\mathbf{r}_t| - c)\mathrm{e}^{\mathrm{j}\phi};\ \phi = \arg(\mathbf{r}_t) \tag{9}$$

The resulting normal force, $\mathbf{f}_{n,s}$, due to support stiffness can be given as follows while avoiding discontinuity at $r = 0$ using arctan functions

$$\begin{aligned} \mathbf{f}_{n,s} &= (k_t\mathbf{f}(\mathbf{r}_e)\mathbf{r}_e + c_t\mathbf{f}(\mathbf{r}_e)\dot{\mathbf{r}}_e)\mathrm{e}^{\mathrm{j}\phi}, \text{ for } \mathbf{r}_e > 0 \\ \mathbf{f}_{n,s} &= 0 \qquad\qquad\qquad\qquad\quad \text{for } \mathbf{r}_e > 0 \end{aligned} \tag{10}$$

with,

$$\mathbf{f}(\mathbf{r}_e) = \left(\frac{1}{\pi}\arctan(\pi\,\gamma_k\,\mathbf{r}_e) + 0.5\right) \tag{11}$$

where, k_t and c_t are the support stiffness and damping coefficients of TDBs; the constant γ_k ensures the continuity of the function $\mathbf{f}(\mathbf{r}_e)$ around $r = 0$. The resulting normal force $\mathbf{f}_{n,c}$ due to contact stiffness is given as

$$\begin{aligned} \mathbf{f}_{n,c} &= \left(k_c\mathbf{f}(\mathbf{r}_e)\mathbf{r}_e^p + b\mathbf{f}\left(\mathbf{r}_e^p\right)\dot{\mathbf{r}}_e^q\right)\mathrm{e}^{\mathrm{j}\phi}, \text{ for } \mathbf{r}_e > 0 \\ \mathbf{f}_{n,c} &= 0 \qquad\qquad\qquad\qquad\qquad\quad \text{for } \mathbf{r}_e > 0 \end{aligned} \tag{12}$$

with, $b = 1.5\lambda k_c$ where, k_c is the contact stiffness of the TDB; λ is the contact parameter. The tangential contact force can be written as

$$\begin{aligned} \mathbf{f}_{t,c} &= \mathrm{j}\mu(v_r)\mathbf{f}_{n,c}e^{j\phi}, \text{ for } \mathbf{r}_e > 0 \\ \mathbf{f}_{t,c} &= 0 \qquad\qquad\qquad\quad \text{for } \mathbf{r}_e > 0 \end{aligned} \tag{13}$$

with sliding velocity,

$$v_r = \frac{(x\dot{y} - y\dot{x})}{\sqrt{x^2 + y^2}} + \omega R \tag{14}$$

and the friction coefficient given as

$$\mu(v_r) = \frac{v_r}{2v_g}\left(\frac{1-\gamma}{1+\zeta|v_r|} + \frac{1+\zeta}{1+\zeta|v_r|^2}\right) \tag{15}$$

with, $\gamma = (1 - \mu_d/\mu_s)^{1/2}$; $\zeta = (1-\gamma)/2v_g\mu_d$. v_g is the regularized parameter. R is the radius of the rotor at TDBs location.

2.4 Overall Equation of Motion of Rotor-AMB System Integrated with TDBs

The assembled equation of motion of rotor-AMB system is given as

$$\mathbf{M}\ddot{\mathbf{r}}(t) + (\mathbf{C}_s + \omega\mathbf{G})\dot{\mathbf{r}}(t) + \mathbf{K}_s\mathbf{r}(t) = \mathbf{f}_e(t) + \mathbf{f}_g - \mathbf{L}_a\mathbf{f}_a - \mathbf{L}_t\left(\mathbf{f}_{n,s} + \mathbf{f}_{n,c} + \mathbf{f}_{t,c}\right) \quad (16)$$

with, $\mathbf{M} = \mathbf{M}_s + \mathbf{M}_d$; $\mathbf{G} = \mathbf{G}_s + \mathbf{G}_d$. Where, $\mathbf{L}_a$ and $\mathbf{L}_t$ are the location matrices of AMBs and TDBs respectively. The equation of motion is utilized to simulate the dropdown analysis of rotor-AMB system and analyze the bearing forces developed in the system under different dynamic conditions.

3 Dropdown Analysis of the Developed System Model

In the events of dropdown, the TDBs absorb the impact of the dynamic loads. The orbit responses from such dropdown events are analyzed to identify the level of impact loads and displacements arising in the system. Also, the analysis is carried out at different operating speed in presence of unbalances. The operational limits and critical TDB location can be identified with the investigation to prevent damage to the machinery.

3.1 Test Rig Description and Simulation Model

The developed finite element model of the rotor system consisting of compressor drive and extension shaft is divided into 75 elements as shown in Fig. 1.

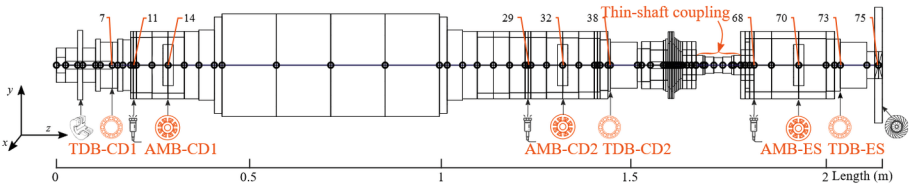

Fig. 1. Wireframe model of the rotor-AMB system with discretized elements. Key nodes such as the AMB actuators, sensors, TDBs and impeller are shown.

The compressor drive is supported on two AMBs at node locations 14 and 32, while the extension shaft is supported by one AMB at node location 70. The touchdown bearings are located at node positions 7, 38 and 73. The displacement at the nodes 11, 29 and 68 are considered for AMB control and at TDBs nodes for the dropdown analysis. An impeller of mass 10 kg is added to the node 75. The equation of motion of the rotor system is solved using SIMULINK model designed on the MATLAB platform to obtain the translational displacements at required nodal positions. The physical parameters of the system are mentioned in Table 1. The Campbell diagram of the rotor-AMB system is shown in Fig. 2. The system is first levitated by the AMBs and then after system is stabilized, the controller is stopped, and the system is allowed to fall on the TDBs under the action of gravity. The displacement responses at the TDBs are analyzed to identify the impact forces generated in the rotor system.

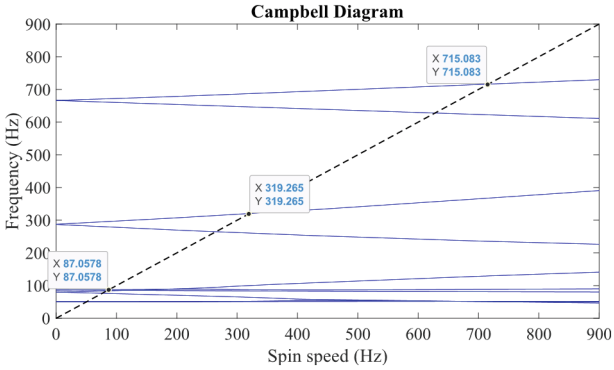

Fig. 2. Campbell diagram of the thin-shaft coupled rotor-AMB system.

Table 1. Physical parameters of the rotor-AMB system integrated with TDBs.

Parameters	Values
Support stiffness (k_t)	1.305e08 N/m
Support damping (c_t)	3.27e03 N-s/m
Contact Stiffness (k_c)	2.02e09 N/m
Power exponents (p and q)	10/9 and 1
Contact parameter (λ)	0.08
Friction coefficients (μ_d); (μ_s)	0.1; 0.2
Continuity parameter (γ_k)	1e11
AMB displacement stiffness factor	7.5e06 N/m
AMB current stiffness factor	735 N/A
Impeller mass and diameter	10 kg and 0.3 m

4 Results and Discussions

Initially, the rotor system is placed on the TDBs at 2e-04 m below the bearing axis as shown in Fig. 3. The system is then levitated by AMBs using the designed LQR controller.

The static load of the rotor system is balanced by the AMBs forces generated due to static control currents as shown in Fig. 3. The system gets stabilized under less than 0.1 s and then after 0.5 s the system is allowed to fall freely on TDBs under the effect of gravity. The dropdown analysis is carried with two different dynamic conditions as mentioned in subsequent sections.

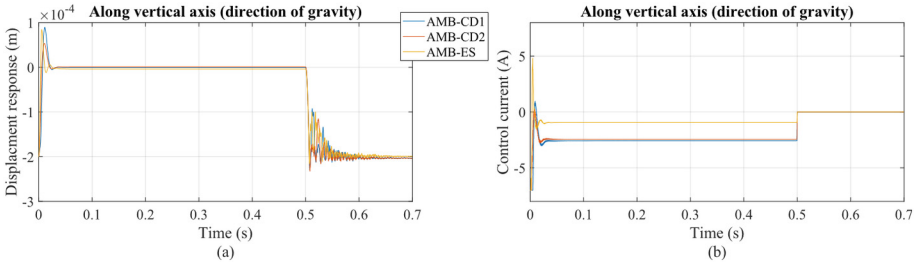

Fig. 3. (a) Displacement and (b) control currents along *y* axis upon levitation.

4.1 Displacement Response for Dropdown at Spin Condition ($\omega = 50$ Hz, Anticlockwise), Without Unbalance

The system is dropped on the TDBs at pure spinning condition, without considering the effect of unbalance in the system. The displacement responses generated in the rotor at the TDBs location are shown in Fig. 4 below. The displacement of the system is scattered along the *x*-axis due to the frictional contact force between the rotor and TDBs. The reaction forces generated at the location of TDBs are in different proportionate due to non-uniform distribution of the gravity load along the shaft axis and the distance between the rotor and TDBs node locations as shown in Fig. 5. The maximum bearing force is generated at the TDB-CD2 is equivalent to 25.6 kN and the selection of TDBs based on load rating must be considered higher than the maximum force value.

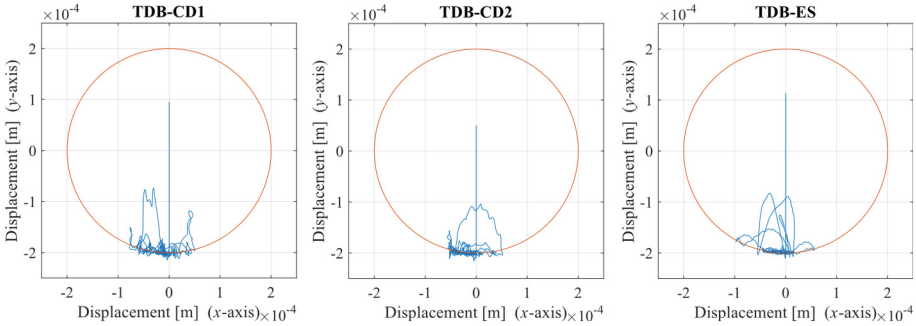

Fig. 4. Displacement response orbits at the TDBs location (speed = 50 Hz).

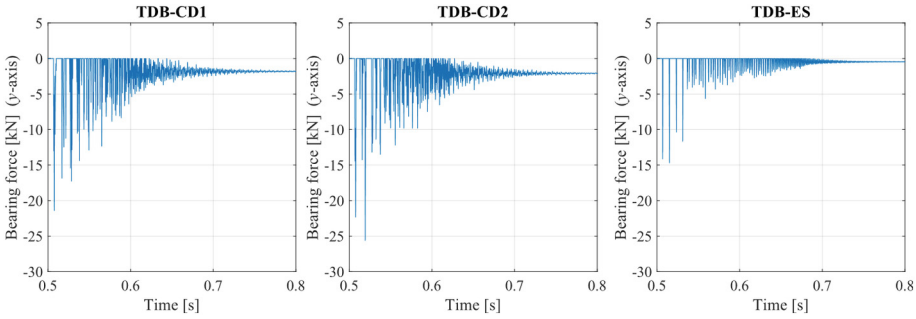

Fig. 5. Plot of the reaction forces at the TDBs location (speed = 50 Hz).

In case the rotor falls while vibrating with different amplitude in presence of unbalances, it would be necessary to analyze the magnitude of bearing force. The effect of unbalance in the system in discussed in the subsequent section.

4.2 Displacement Response for Dropdown at Spin Condition (ω = 50 Hz, 100 Hz and 150 Hz Anticlockwise), with Unbalance

With the inclusion of unbalance in the system, the amplitude of vibration effects the intensity of the reaction forces. Also, the number of bounce off of rotor increases, which in turn increases the stress cycles the TDBs are required to withstand. The acceleration of rotor at the time of release and the direction of motion affects the intensity of the reaction forces. For the rotor with centre of mass above the bearing axis at the time of dropdown, the reaction force is higher at TDBs as the distance between the rotor and the TDBs increases. The analysis is carried out for an unbalanced system in which an additional unbalance is added with G 2.5 grade to show the effect of unbalance on the system. Therefore, the unbalance magnitude of 500 g-mm is assumed at the impeller corresponding to node 75. The bearing forces at the TDBs of the system released with different phase of unbalances from 0 to 360° (with step of 22.5°) is shown in Fig. 6. The maximum force of 28.9 kN is observed at TDB-CD2 along vertical (y) axis and 7.8 kN at TDB-ES for horizontal (x) axis. The TDBs are required to withstand several numbers of bounce off during dropdown. The number of bounce off of rotor with bearing load above 10 kN with variation in phase of unbalance is also estimated as mentioned in Table 2. The maximum number bounce off i.e., 20 is observed for TDB-CD1 at the compressor drive side.

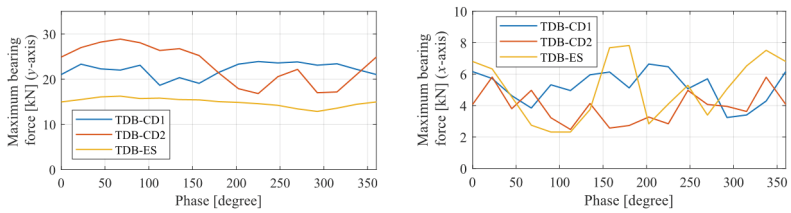

Fig. 6. Maximum force at the TDBs with unbalance phase (0–360°) along (a) y and (b) x axes. (c) Number of bounce off at TDBs for bearing load above 10 kN with unbalance phase (0–360°) along y axis (spin speed = 50 Hz).

Table 2. Estimated Bearing forces and the number of bounce off at the TDBs location with different operating speed (50, 100, 150 Hz) of the rotor system.

Frequency (Hz)	TDB Bearing forces (kN)	Bearing forces (kN)		Bounce offs
		y-axis	*x*-axis	
50	TDB-CD1	23.9	6.6	20
	TDB-CD2	28.9	5.8	14
	TDB-ES	16.3	7.8	6
100	TDB-CD1	34.2	10.6	18
	TDB-CD2	33.5	9.5	14
	TDB-ES	25.0	14.2	15
150	TDB-CD1	26.1	8.3	23
	TDB-CD2	27.6	8.9	22
	TDB-ES	22.7	16.6	53

The same procedure is performed for spin speeds of 100 and 150 Hz to check the severity in the reaction forces and bounce off with change in phase of unbalance during dropdown. The orbit plot of displacement response for dropdown event at operating speed of 150 Hz is shown in Fig. 7. The amplitude of the displacement due to unbalance is higher at the TDB-ES. As a result, the number of bounce off with higher bearing load is greater at TDB-ES location as shown in Fig. 8. It can be seen from the Table 2 that in case of dropdown in different dynamic condition, the maximum forces are around 34.2 kN at TDB-CD1.

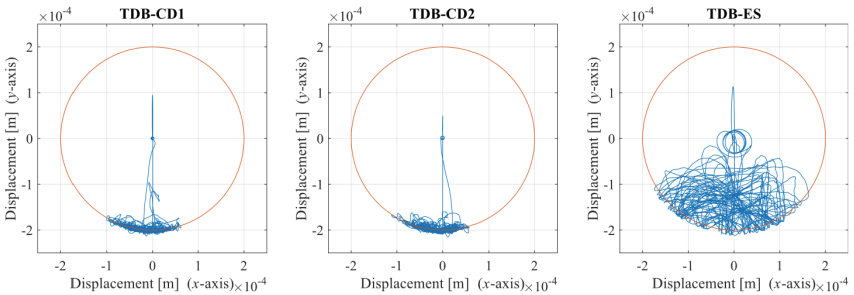

Fig. 7. Displacement response orbits at the TDBs location (speed = 150 Hz).

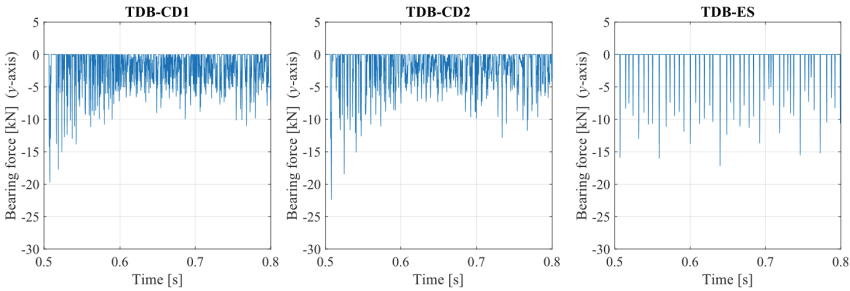

Fig. 8. Plot of reaction forces at the TDBs location (speed = 150 Hz).

There is an increment in the magnitude of bearing forces along x-axis due to increase in amplitude of vibration with spin speed. However, the number of bounce off is increased up to 53 at the TDB-ES location due to increase in the amplitude of vibration. The rotor remains bouncing off in TDB until the operating speed of the system is reduced to zero or the system is switched off. The excessive bounce off of rotor may result in the failure of the TDB-ES at high-speed condition.

5 Conclusions

The dropdown analysis of the 3 AMB-rotor system in event of rotating condition with different operating speed and unbalance force is carried out. The maximum force generated at the TDBs is critical at the compressor drive side at different operating speed with unbalance. However, at higher speed due to increase in vibration amplitude at the extension shaft, the number of bounce off increases at TDB-ES. As a result of this, the TDB at extension shaft is subjected to large magnitude of repetitive load and increase its chances of failure in dropdown event. Therefore, the presence of unbalance has significant effect in identifying the critical TDB in the dropdown event for high speed coupled rotor-AMB systems. Also, when heavier loads are in extension shaft side possible failures of TDBs occurs more on extension shaft side. That can be considered in the design of extension shaft on maintenance point of view.

References

1. Gerada, D., Mebarki, A., Brown, N.L., Gerada, C., Cavagnino, A., Boglietti, A.: High-speed electrical machines: Technologies, trends, and developments. IEEE Trans. Industr. Electron. **61**(6), 2946–2959 (2013)
2. Uzhegov, N., Smirnov, A., Park, C.H., Ahn, J.H., Heikkinen, J., Pyrhönen, J.: Design aspects of high-speed electrical machines with active magnetic bearings for compressor applications. IEEE Trans. Industr. Electron. **64**(11), 8427–8436 (2017)
3. Kurvinen, E., et al.: Design and manufacturing of a modular low-voltage multimegawatt high-speed solid-rotor induction motor. IEEE Trans Ind App **57**(6), 6903–6912 (2021)
4. Pyrhönen J, et al.: An electric machine system. Worldwide Appl. WO2022258880A1 (2022)
5. Saket, F., Sahinkaya, M., Keogh, P.: Measurement and calibration of rotor/touchdown bearing contact in active magnetic bearing systems. Mech. Syst. Signal Process. **122**, 1–18 (2019)

6. Neisi, N., Heikkinen, J., Sillanpää, T., Hartikainen, T., Sopanen, J.: Performance evaluation of touchdown bearing using model-based approach. Nonlinear Dyn. **101**(1), 211–232 (2020). https://doi.org/10.1007/s11071-020-05754-9
7. Jarroux, C., Mahfoud, J., Defoy, B., Alban, T.: Stability of rotating machinery supported on active magnetic bearings subjected to base excitation. J. Vibr. Acoust. **142**(3), 031,004 (2020)
8. Pesch, A.H., Sawicki, J.T.: Active magnetic bearing online levitation recovery through μ-synthesis robust control. Actuators, MDPI **6**, 2 (2017)
9. Lyu, M., Liu, T., Wang, Z., Yan, S., Jia, X., Wang, Y.: Orbit response recognition during touchdowns by instantaneous frequency in active magnetic bearings. J. Vibr. Acoust. **140**(2) (2018)
10. Liu, T., Lyu, M., Wang, Z., Yan, S.: An identification method of orbit responses rooting in vibration analysis of rotor during touchdowns of active magnetic bearings. J. Sound Vib. **414**, 174–191 (2018)
11. Jastrzebski, R.P., Putkonen, A., Kurvinen, E., Pyrhönen, O.: Design and modeling of 2 MW AMB rotor with three radial bearing-sensor planes. IEEE Trans. Ind. Appl. **57**(6), 6892–6902 (2021)
12. Jarroux, C., Mahfoud, J., Dufour, R., Legrand, F., Defoy, B., Alban, T.: Investigations on the dynamic behaviour of an on-board rotor-AMB system with touchdown bearing contacts: modelling and experimentation. Mech. Syst. Signal Process. **159**(107), 787 (2021)